

See discussions, stats, and author profiles for this publication at: <https://www.researchgate.net/publication/227581685>

Solution structure of the catalytic domain of human stromelysin complexed with a hydrophobic inhibitor

ARTICLE *in* PROTEIN SCIENCE · DECEMBER 1995

Impact Factor: 2.85 · DOI: 10.1002/pro.5560041205 · Source: PubMed

CITATIONS

48

READS

13

7 AUTHORS, INCLUDING:



[Steven R Van Doren](#)
University of Missouri
60 PUBLICATIONS **1,390** CITATIONS

[SEE PROFILE](#)



[Weidong Hu](#)
City of Hope National Medical Center
72 PUBLICATIONS **2,558** CITATIONS

[SEE PROFILE](#)



[Erik Roelpeter Zuiderweg](#)
University of Michigan
147 PUBLICATIONS **6,779** CITATIONS

[SEE PROFILE](#)

Solution structure of the catalytic domain of human stromelysin complexed with a hydrophobic inhibitor



STEVEN R. VAN DOREN,^{1,2} ALEXANDER V. KUROCHKIN,¹ WEIDONG HU,¹
QI-ZHUANG YE,³ LINDA L. JOHNSON,³ DONALD J. HUPE,³ AND
ERIK R.P. ZUIDERWEG^{1,4}

¹ Biophysics Research Division, The University of Michigan, Ann Arbor, Michigan 48109-1055

² Department of Biochemistry, University of Missouri-Columbia, Columbia, Missouri 65211

³ Department of Biochemistry, Parke-Davis Pharmaceutical Research, Division of Warner-Lambert Company, Ann Arbor, Michigan 48105

⁴ Department of Biological Chemistry, The University of Michigan Medical School, Ann Arbor, Michigan 48109-0606

(RECEIVED July 27, 1995; ACCEPTED September 25, 1995)

Abstract

Stromelysin, a representative matrix metalloproteinase and target of drug development efforts, plays a prominent role in the pathological proteolysis associated with arthritis and secondarily in that of cancer metastasis and invasion. To provide a structural template to aid the development of therapeutic inhibitors, we have determined a medium-resolution structure of a 20-kDa complex of human stromelysin's catalytic domain with a hydrophobic peptidic inhibitor using multinuclear, multidimensional NMR spectroscopy. This domain of this zinc hydrolase contains a mixed β -sheet comprising one antiparallel strand and four parallel strands, three helices, and a methionine-containing turn near the catalytic center. The ensemble of 20 structures was calculated using, on average, 8 interresidue NOE restraints per residue for the 166-residue protein fragment complexed with a 4-residue substrate analogue. The mean RMS deviation (RMSD) to the average structure for backbone heavy atoms is 0.91 Å and for all heavy atoms is 1.42 Å. The structure has good stereochemical properties, including its backbone torsion angles. The β -sheet and α -helices of the catalytic domains of human stromelysin (NMR model) and human fibroblast collagenase (X-ray crystallographic model of Lovejoy B et al., 1994b, *Biochemistry* 33:8207–8217) superimpose well, having a pairwise RMSD for backbone heavy atoms of 2.28 Å when three loop segments are disregarded. The hydroxamate-substituted inhibitor binds across the hydrophobic active site of stromelysin in an extended conformation. The first hydrophobic side chain is deeply buried in the principal S_{1'} subsite, the second hydrophobic side chain is located on the opposite side of the inhibitor backbone in the hydrophobic S_{2'} surface subsite, and a third hydrophobic side chain (P_{3'}) lies at the surface.

Keywords: catalytic domain; hydroxamate; matrix metalloproteinase 3; multidimensional NMR; protein structure; stromelysin

As a member of the zinc- and calcium-dependent family of matrix metalloproteinases (MMPs), which hydrolyze the extracellular matrix, stromelysin participates in the tissue remodeling of health and disease. Regarding the shared domain structure of the MMPs, their subfamilies, specificity, transcriptional regulation, activation, and posttranslational regulation, see reviews of Woessner (1991), Matrisian (1992), Birkedal-Hansen et al. (1993), and Nagase (1995). The involvement of MMPs in tissue remodeling includes that of development, tissue resorption, reproduction, angiogenesis, and wound healing, and that of sev-

eral diseases including arthritis and cancer. The invasive potential of human tumors is correlated with the expression of several MMPs (Stetler-Stevenson et al., 1993) but the particular MMPs expressed vary among types of tumors. Highly elevated levels of stromelysin (MMP-3), alongside other MMPs, have been measured in many carcinomas of the breast, bone, and esophagus (Clavel et al., 1992; Sasaguri et al., 1992; Shima et al., 1992). MMP-3 plays a principal role in joint destruction as well. The concentration and proteolytic activity of stromelysin have been found to be elevated dramatically in joints afflicted by either osteoarthritis (Okada et al., 1992; Wilhelm et al., 1993) or by rheumatoid arthritis (Okada et al., 1989; Gravallese et al., 1991; Firestein & Paine, 1992; Walakovits et al., 1992). Consequently, stromelysin and other MMPs are drug targets for which

Reprint requests to: Erik R.P. Zuiderweg, Biophysics Research Division, The University of Michigan, 930 North University Avenue, Ann Arbor, Michigan 48109-1055; e-mail: erpz@ernst.biop.umich.edu.

atomic resolution structures have been sought to aid the drug design process.

A representative of the MMPs, the catalytic domain of human stromelysin was shown by NMR to contain three helices and a five-stranded mixed β -sheet (Gooley et al., 1993; Van Doren et al., 1993), organized in a fold similar to that of crayfish astacin (Bode et al., 1992). The zinc-binding motif at the active site, containing the conserved HEXXHXXGXXH sequence, as well as a conserved methionine in a turn adjacent to the catalytic zinc, are also shared with astacin. These structural features, shared not only among the matrix metalloproteinases and astacins, but also among the serralysins and adamalysins, allow them to be grouped into a superfamily dubbed the metzincins (Bode et al., 1993). In efforts to aid drug design, crystallographic structures of the catalytic domain of fibroblast collagenase or MMP-1 (Borkakoti et al., 1994; Lovejoy et al., 1994a, 1994b) and of neutrophil collagenase or MMP-8 (Bode et al., 1994; Reinemer et al., 1994; Stams et al., 1994) have become available. The structure of full-length porcine MMP-1 shows that the C-terminal hemopexin-like domain is a four-bladed “ β propeller” (Li et al., 1995). An NMR solution structure of stromelysin catalytic domain at pH 5.5 complexed with an *N*-carboxy alkyl inhibitor, *N*-(*R*-carboxy-ethyl)- α -(*S*)-(2-phenyl ethyl)-glycyl-L-arginine-*N*-phenyl amide, has been published as well (Gooley et al., 1994), and has since been further refined (Protein Data Bank access code 2SRT).

We present here the solution structure of human stromelysin’s catalytic domain under conditions of higher calcium affinity (pH 7.0), and concentration, complexed with a hydroxamate inhibitor of more hydrophobic character ((*R,S*)-*N*-[2-[2-(hydroxamino)-2-oxoethyl]-4-methyl-1-oxopentyl]-L-leucyl-L-phenylalaninamide; DiPasquale et al., 1986) and in the presence of acetonitrile as a co-solvent. Our solution structure of the catalytic domain of human stromelysin reveals the binding mode of this peptide substrate analogue in the hydrophobic pockets of the active site (Kinemages 1 and 2) (Protein Data Bank access codes 1UMT and 1UMS).

Results

Assignments

The backbone assignments and secondary structure were previously reported by Van Doren et al. (1993). The bulk of ^1H and ^{13}C side-chain assignments were obtained using cross-polarization-driven HCCH-TOCSY spectra (Majumdar et al., 1993). CBCA (CO)NH (Grzesiek & Bax, 1992) and HBHA(CO)NH (Grzesiek & Bax, 1993) experiments proved helpful in correlating backbone and side-chain groups. Due to short T_2 s in general for this protein and for the methylene groups in particular, assignment of methylene groups was problematic, but a 3D HCH (Yamazaki et al., 1993) with semi-constant time enhancements proved very helpful in such cases. For the most difficult of methylene assignments and for connecting aromatic ring systems, ^{15}N - and ^{13}C -resolved NOESY spectra were employed. The bulk of the assignments, however, were obtained from scalar correlations. The assignments are currently more than 90% complete. Stereospecific valine and leucine methyl assignments of the protein, but not inhibitor, were obtained from a [^{13}C]HSQC spectrum of a 10% uniformly ^{13}C -labeled sample (Neri et al., 1989). Protein-protein NOE assignments were obtained from 3D heteronuclear-resolved NOESY experiments (Fesik & Zuiderweg, 1988; Marion et al., 1989). In particular, ^{15}N -resolved NOESY (as described by Van Doren et al. [1993]) and ^{13}C -resolved NOESY (as modified by Majumdar & Zuiderweg [1993]) spectra acquired in H_2O using gradient enhancements and mixing times of 70 ms were used. Protein-protein NOE assignments also relied upon a 3D ^{13}C -resolved NOESY (as modified by Van Doren & Zuiderweg [1994]) collected in D_2O with a mixing time of 55 ms. Assignments of the peptide-derived inhibitor relied on a TOCSY (Bax et al., 1994) and on a NOESY (Ikura & Bax, 1992), which suppress virtually all ^{13}C -bound proton signals from the uniformly $^{13}\text{C}/^{15}\text{N}$ -labeled stromelysin in order to reveal the ^{12}C -bound protons of the unlabeled, hydroxamate-substituted peptide-like inhibitor. The inhibitor assignments were supplemented by a $^{13}\text{C}/^{15}\text{N}$ -filtered NOESY (modified from Ikura & Bax [1992]) of the same sample in H_2O . These NOESY spectra, suppressing the ^{13}C - and ^{15}N -bound protons of the protein (NOESY mixing times of 100 ms), were used in conjunction with the previously mentioned 3D NOESY spectra of shorter mixing times for identifying protein-inhibitor NOEs.

The fold

The amino-terminus of mature stromelysin lies along the third helix (C) of the catalytic domain and leads into β -strand I (the secondary structure elements are defined in the legend to Fig. 1; strands are shown as flat strips in Fig. 1 and in yellow in Fig. 2; Kinemage 2) of the mixed β -pleated sheet. Strand I is terminated by a bulge that precedes an extended segment of a loop, parallel to the sheet but not hydrogen bonded to the sheet. The loop turns back into the long and perfectly amphipathic helix A (shown in white in Fig. 2). A short loop then turns back immediately to connect to β -strand II at the edge of the sheet. Thus, parallel strands I and II and helix A form a classic right-handed β - α - β motif. From the end of strand II, a loop crosses over strand I on the convex side of the sheet leading to strand III running parallel to and between stands I and V. From strands III to IV, an S-shaped loop traverses the convex side of the sheet. The first or upper lobe of the S shares in coordinating the structural zinc ion (white sphere in Fig. 2), whereas the second or lower lobe binds a structural calcium ion (blue sphere in Fig. 2; Kinemage 2). Following this loop at the edge of the β -sheet, strand IV runs (antiparallel to strand V) along the active site cleft it borders. Strand V, sandwiched between strands III and IV, provides a histidyl nitrogen ligand to the structural zinc ion as does strand IV. Altogether, the sheet is amphipathic with the exposed regions of the convex side being hydrophilic and the concave interior being hydrophobic. Strands II, I, III, and V run parallel in that order.

A portion of the loop joining strand V with helix B borders the active site. The central helix B is mostly buried and crosses helix A with an angle of about 42°. Helix B lines the bottom of the active site cleft. The C-terminal end of helix B contributes two histidines, which coordinate the Zn involved in catalysis (white ball in Fig. 2; Kinemage 2). The third histidine ligand to this zinc is positioned a few residues away in the long loop connecting the B helix with the C helix. Met 219, conserved throughout the greater family of “metzincin” zinc endopeptidases, lies adjacent to the active site histidines. A few residues from this methionine is an extended sequence of hydrophobic residues that forms the wall of the active site cleft opposite the wall of the cleft

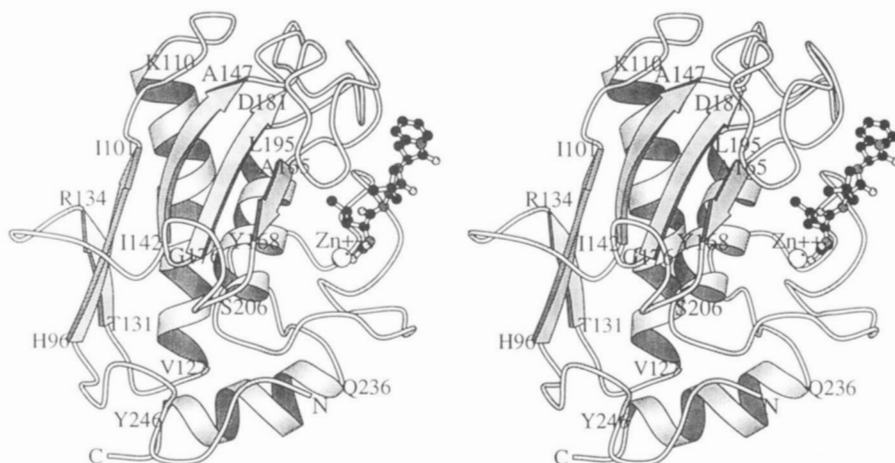


Fig. 1. Topology of the stromelysin catalytic domain. Flattened arrows represent the β -strands and wound arrows represent α -helices. A ball-and-stick plot represents the heavy atoms of the inhibitor (ICI U24522; DiPasquale et al., 1986) comprised of a hydroxamate residue followed by an isobutyl-containing residue, a leucine, and a phenylalaninamide. (Systematic name: (*R,S*)-*N*-(2-[2-(hydroxamino)-2-oxethyl]-4-methyl-1-oxopentyl)-*l*-l eucyl-*l*-phenylalaninamide.) The catalytic zinc ion is represented by a white sphere, carbon atoms by black spheres, nitrogen atoms by medium gray spheres, and oxygen atoms by light gray spheres. The average structure subjected to minimization with restraints was plotted using MOLSCRIPT (Kraulis, 1991). The first and last residues of each of the five β -strands (I–V) and three α -helices (A–C) are shown as follows: I (H96–I101); II (T131–R134); III (I142–A147); IV (A165–Y168); V (G176–D181); A (K110–V127); B (L195–S206); and C (Q236–Y246).

formed by strand IV. The loop continues to where it makes hydrophobic contacts with helix A. Ser 235 likely serves as the N residue and D238 as the N + 3 residue of an N-capping box of helix C (having reciprocal side-chain to backbone amide hydrogen bonds), judging from the characteristic upfield shifted $^{13}\text{C}\alpha$ and downfield-shifted $^{13}\text{C}\beta$ resonances as described by Gronenborn and Clore (1994) to be indicative of such structures. Helix C lies along the surface of the domain at an angle of roughly 80° relative to helix A. Helix C has a few breaks in medium range NOEs and in protection of amides from exchange (i.e., of G241 and S244) and some irregularity of backbone torsion angles. The C-terminal eight residues of the catalytic domain studied are disordered and have been omitted from calculations of the ensemble.

Precision

The mean RMS deviation (RMSD) among the ensemble of 20 structures to the average structure for backbone heavy atoms is 0.91 ± 0.06 Å and for all heavy atoms is 1.42 ± 0.06 Å (see Kinemage 1). Regions of lowest RMSD (Fig. 3) are correlated with the regions for which the most medium- and long-range NOE (histogram of Fig. 4; Table 1) constraints are available. The number of such NOE distance restraints is correlated with the occurrence of regular secondary structure and with the degree of burial in the hydrophobic core. Most of the regions of regular secondary structure have backbone RMSDs (from the average structure) of less than 0.6 Å. The helices can be identified in Figure 4 by the presence of medium-range NOEs.

Angular order parameter statistics (Fig. 5; Hyberts et al., 1992) suggest most backbone torsions are well defined to the extent that the ϕ and ψ order parameters exceed 0.8, a threshold reflecting a standard deviation of less than 38° , for the given dihedral angle throughout the ensemble. Portions of four loops in the model have multiple residues with order parameters below this threshold: amino-terminal residues 83–94; residues 147–

156 of the III–IV metal-binding loop; residues 188–192 of the V–B loop; and residues 208–232 of the B–C loop. The higher positional RMSDs are found in these regions as well. These regions are correlated with surface exposure and higher amide ex-

Table 1. Summary of restraints used in structure calculations

Restraint type	Number of restraints
Assigned NOE crosspeaks used in calculations ^a	1,386
Total NOE distance restraints	1,336
Total protein–protein NOE distance restraints	1,281
Intraresidue	3
Sequential ($ i - j = 1$)	510
Medium range ($2 \leq i - j \leq 4$)	302
Long range ($ i - j > 4$)	466
Total inhibitor NOE distance restraints	55
Sequential and $ i - j = 2$	3
Long range inhibitor–protein	52
Mean deviation above all NOE upper bounds, Å	0.037 ± 0.001
Mean largest NOE violation, Å	0.64 ± 0.07
Dihedral angle (ϕ) restraints	55
Hydrogen bond distance restraints (2 per H-bond)	84
Total metal–ligand distance restraints	15
Zinc–nitrogen	6
Zinc–oxygen	3
Calcium–oxygen	6

^a In 50 cases, NOEs were present to both geminal protons of a methylene group or to both methyl groups of a side chain, but only one (rather than two) restraint could be used. That is, due to a software limitation, a single restraint was defined to the pseudoatom defined for the given group rather than properly to both constituents of the pseudoatom. This accounts for the difference of 50 between the number of assigned cross-peaks and NOE restraints used.

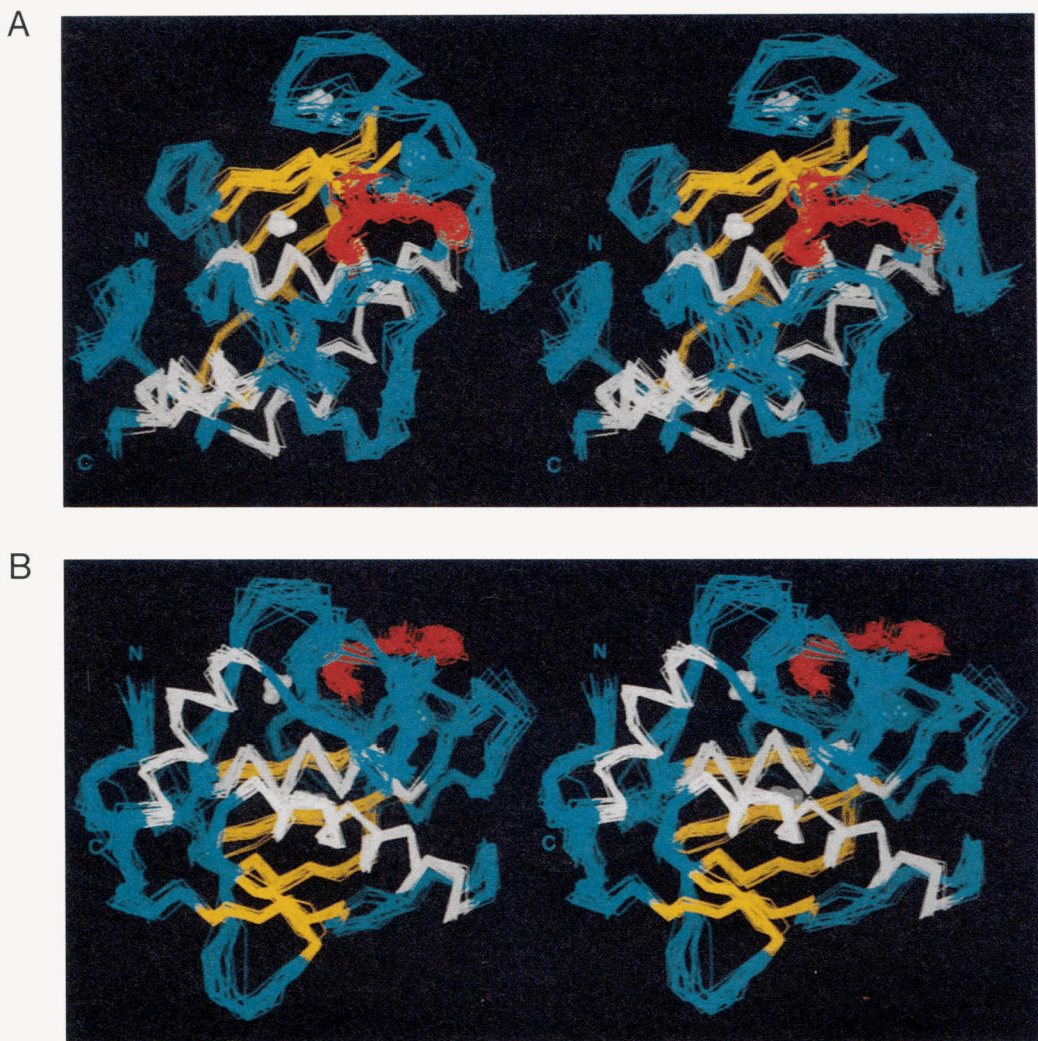


Fig. 2. **A:** Ensemble of the 20 accepted structures of the catalytic domain of stromelysin represented by their C_α traces. Heavy atoms of the bound substrate analogue, apart from the hydroxamate group, are displayed in red. Helices are depicted in white and β -strands in yellow. The catalytic helix B runs in the plane of the page with N- to C-terminal ends running right to left. **B:** Rotation of 90° about helix B relative to that shown in A.

change rates resulting in missing assignments or degeneracy and fewer structural restraints. The last 8 residues of the 174-residue domain are dynamically disordered, evident by their longer T₂ values, and have been omitted from the model.

Stereochemical quality

An evaluation using PROCHECK (Laskowski et al., 1993) reveals that the contacts, hydrogen bonding energies, and side-chain rotamers are typical of the quality of 2.5-Å crystallographic structures or better. Peptide bond planarity and C_α chirality are satisfactory as well. The members of the ensemble on average have 87% of their non-glycine, non-proline residues in allowed regions of the Ramachandran map. On average, 9% of a member's residues are in marginally allowed regions of the Ramachandran plot and 4% are in disallowed regions. Wagner and coworkers have demonstrated that poor backbone dihedral angles in NMR solution structures cluster at residues whose tor-

sions are less reproducible across the ensemble, i.e., having lower backbone angular order parameters (cf. Hyberts et al., 1992). The best defined residues with angular order parameter in excess of 0.9 (corresponding to a standard deviation for the torsion angle of <25°) have conformationally orthodox backbone dihedral angles as shown in the Ramachandran plot for all 20 members of the ensemble (Fig. 6). The occurrences with positive ϕ in the middle of the upper right quadrant belong to Gly 159 and Gly 161 (20 points each) of a calcium binding site.

Inhibitor binding

The inhibitor runs antiparallel to strand IV (in Fig. 7 and Kine-mages 1 and 2, top to bottom for "N- to C-") with an extended conformation, having medium to strong d_{αN} sequential NOEs. The *i*-butyl side chain of the residue lacking an amide packs deeply (away from the viewer) into the very deep and hydrophobic S'₁ subsite where it (particularly its methyl groups) has

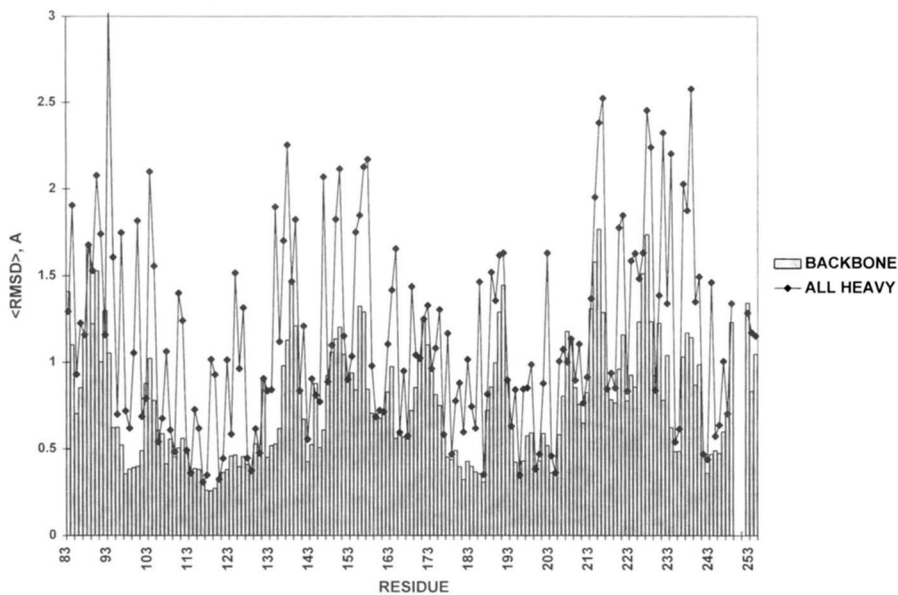


Fig. 3. Mean RMSD (\AA) to the average structure among the 20 accepted structures of stromelysin catalytic domain. RMSDs for all heavy atoms of each residue are indicated by diamonds connected with lines. RMSDs for the backbone heavy atoms (N, CA, C', O) of each residue are shown using gray bars. Inhibitor positions occupy the last three positions (252–254) in the plot, following the break after protein residue 248.

NOEs to Leu 164, Val 198, His 201, Pro 221, Leu 222, and Tyr 223. The P'₂ leucine residue fits into the broad, shallow S'₂ hydrophobic subsite at the surface where it has NOEs to Asn 162, Val 163, Leu 164, Ala 165, and Leu 222. The lack of stereospecific methyl assignments for the unlabeled inhibitor limits its precision in the model. The phenylalaninamide at P'₃ occupies a shallow notch where it has NOEs to Val 163, Leu 164, Thr 190, Thr 191, Thr 193, Leu 222, Tyr 223, and His 224.

Discussion

Terminal regions

The location of the amino-terminus varies significantly among the crystallographic and NMR structural models of matrix me-

taloproteinases recently reported. Reported locations include: in the active site of a neighboring protease molecule (Lovejoy et al., 1994b); in its own active site (Gooley et al., 1994); pointing away into “solution” (i.e., the crystal) (Bode et al., 1994; Borkakoti et al., 1994; Stams et al., 1994); and along the carboxy-terminal helix C (Lovejoy et al., 1994a; Reinemer et al., 1994). Like the latter two reports, the mature N-terminus (Phe 83) of the catalytic domain of stromelysin in this NMR model runs along the surface of helix C. Reinemer et al. (1994) reported that the amino group of the N-terminal phenylalanine forms a salt bridge with the fully conserved Asp 232 in neutrophil collagenase properly processed at the correct N-terminal residue to give full activity. This work suggests the disordered and divergent locations of the N-termini in the structural models of MMPs is caused in part by the differences in N-terminal starting positions

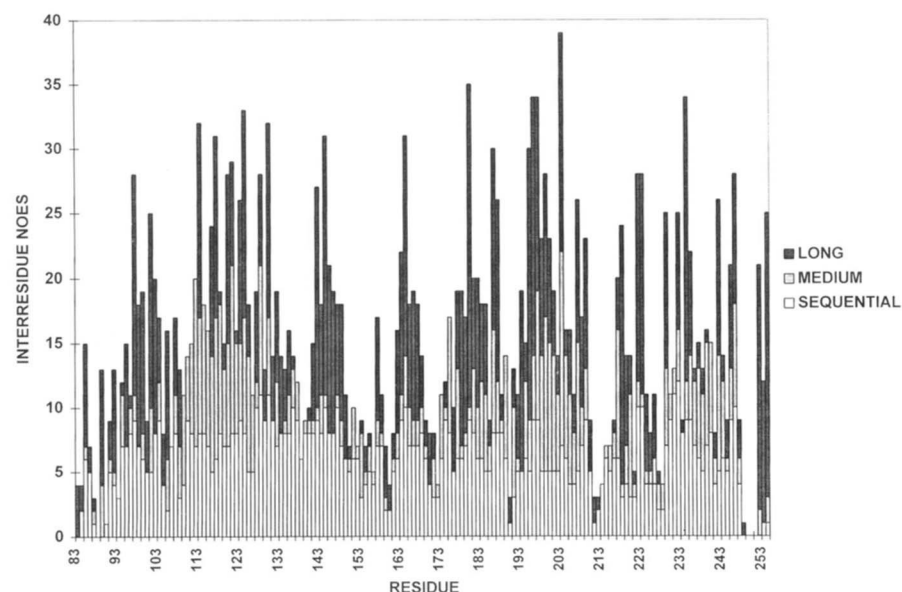


Fig. 4. Histogram of the number of interresidue NOE distance restraints used for each residue in the structure calculations. NOEs are separated into classes as long-range (dark), medium-range (medium), or sequential (light). The 50 NOEs discussed with reference to the first two rows of Table 1 are excluded from this tally. NOEs appear for both residues involved. The inhibitor positions occupy the last three positions in the plot.

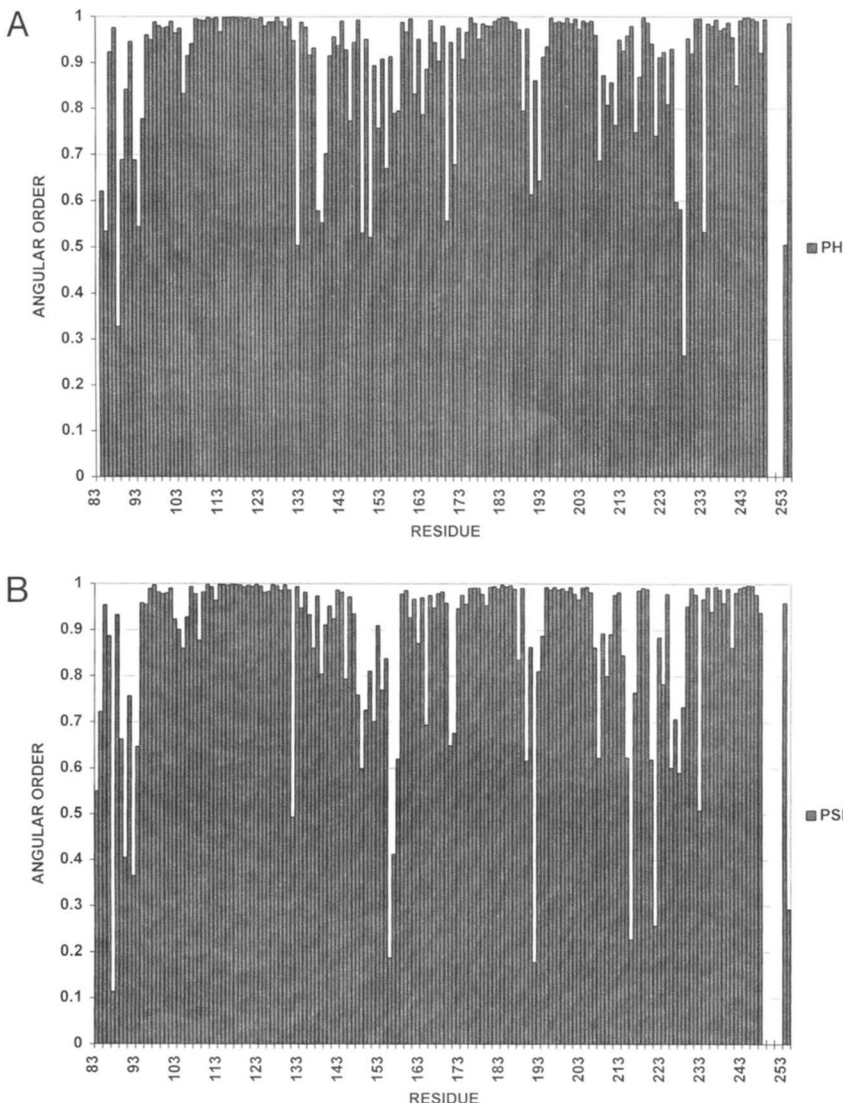


Fig. 5. Histogram plotting angular order parameters (Hyberts et al., 1992) for ϕ (**A**) and ψ (**B**) backbone torsion angles. Standard deviations of a torsion angle of 10, 20, 40, and 80° correspond to angular order parameters of 0.985, 0.942, 0.768, and 0.397, respectively.

of the domains used in such studies. The stromelysin domain used here has been found by N-terminal sequencing to begin at the “correct” residue. Because some of the members of this NMR ensemble have a distance of 5.5–7 Å between Phe 83 and Asp 237 (without use of electrostatic terms in the restrained molecular dynamics to draw this closer in our model), it is quite plausible that properly processed stromelysin also has the same salt bridge between the amino-terminal phenylalanine and the equivalent aspartate.

Role of metal

As stromelysin catalytic domain is most active at pH 6.0 (Ye et al., 1992), a logical choice would be to study the molecule at or near that pH, similar to the work reported by Gooley et al. (1994). However, we have observed that, at pH 6.0, a large number of very sharp lines develops quickly at random coil proton chemical shifts in the NMR spectrum of inhibited stromelysin catalytic domain. The sharp lines can be made to reversibly disappear by adjusting the pH to 7.0 and by increasing the concen-

tration of Ca^{2+} ions in the buffer. These lines therefore cannot correspond to products of autolytic cleavage, but must represent unfolded areas of the protein. It was decided to study stromelysin at pH 7, in the presence of 20-fold excess of CaCl_2 to avoid the [local] unfolding. Stromelysin activity is just a factor of two lower than optimum at pH 7 (Ye et al., 1992). We speculate that the unfolding at pH 6.0 occurs in the Ca^{2+} binding site regions because Ca^{2+} affinity is known to decrease 10-fold with a pH change from 7 to 5.5 (Wilhelm et al., 1993). At least two calcium ions bind to stromelysin, as was determined by mass spectrometry (Hu et al., 1994). It is expected that they play an analogous role in stabilizing the β -sheet as in collagenase, where X-ray diffraction studies identified clusters of acidic residues coordinating the metal ions in these regions (Lovejoy et al., 1994b). The current NMR study reveals one such cluster of conserved acidic residues in stromelysin by the NOEs of the side chain of Glu 184 with the side chains of both Asp 158 and Asp 181. This cluster bridges the loop between strands III and IV with the loop at the C-terminal end of strand V. A second cluster of conserved carboxylate-containing residues, Asp 107 and Asp 182, are in

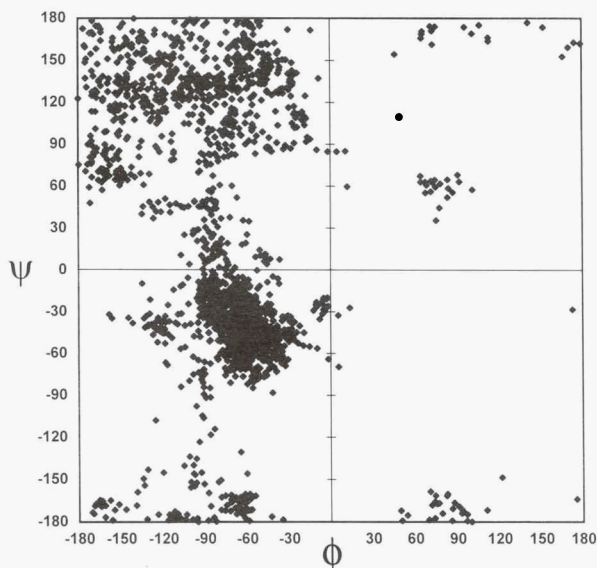


Fig. 6. Ramachandran plot for the residues of all 20 members of the ensemble whose angular order parameters for both ϕ and ψ exceed 0.9.

NOE contact and join the strand I to helix A loop with the strand V to helix B loop. These two respective clusters of negative charge are the probable binding sites for one Ca^{2+} ion each as a high electrostatic energy cost would be imposed if calcium

were absent from each of these two sites. At the first calcium site in the loop between strands III and IV, NOEs from the backbone of conserved Gly 159, conserved Gly 161, and Val 163 to either of the calcium-binding Asp 158 or Glu 184 residues are consistent with the crystallographic observation of three additional calcium-binding carbonyl groups. These are the carbonyl oxygens of the equivalent two glycines and asparagine of fibroblast collagenase (MMP-1; Lovejoy et al., 1994a). Because the six distances of calcium to ligand at this site, ranging from 1.8 to 2.5 Å, reported by Lovejoy et al. (1994a) are consistent with the NOE data, they have been included in this model. Some crystallographic models of collagenase include a third calcium ion just beyond the opposite edge of the sheet between the loops feeding into the N-terminal ends of β -strands III and V.

A structural zinc also stabilizes the β -sheet. A structural zinc, in addition to the catalytic zinc ion, was found by Salowe et al. (1992). The two conserved histidines of strands IV and V, His 166 and His 179, adjacent and in NOE contact on the convex side of the sheet were implicated in ligation of this zinc (Gooley et al., 1993; Van Doren et al., 1993). From the loop joining strands III and IV a third histidine, His 151, was also found to coordinate this zinc on the basis of its imidazole assignments and NOEs (Gooley et al., 1993, 1994). Because Asp 153 is in NOE contact with His 151 and is fully conserved, it is the best candidate to provide the fourth ligand to complete an ordinary tetrahedral coordination geometry. The recent X-ray structures have confirmed these observations, and the metal-ligand distances reported by Lovejoy et al. (1994a) have been included in

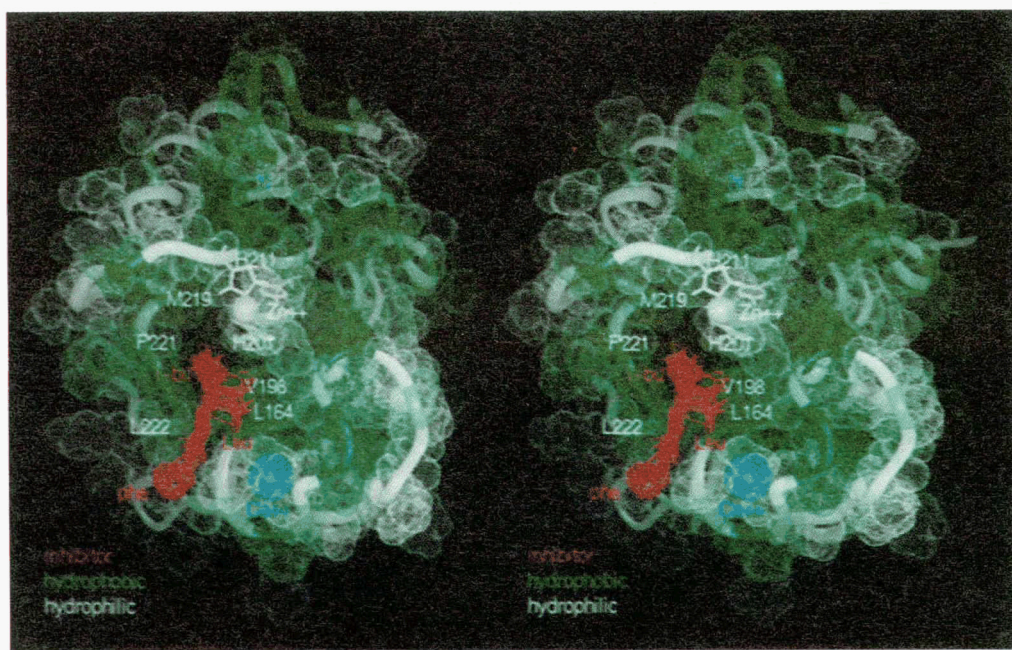


Fig. 7. Van der Waals surface plot of the average structure minimized with restraints displays the hydrophobic active site with bound drug from all 20 structures colored red. The catalytic zinc ion (white sphere) is in the center and the structural calcium ion near the primed subsites is near the bottom (light blue sphere). A ribbon runs through the protein C α coordinates. In order to highlight the hydrophobicity of the active site region, the hydrophobic protein residues are colored green and the hydrophilic residues are colored white and the glycine and tyrosine residues of intermediate hydrophobicity are colored light green. The superimposition used was an all-heavy atom superimposition for the entire protein-drug complex. In order to display the deep S_{1'} subsite, the hydroxamate residue has been omitted from the heavy atom plot of the ensemble of inhibitor conformations. Val 163 is obscured from view underneath the first two residues of the inhibitor shown.

this model. β -Strand IV and the loop immediately preceding, rigidified by the distal Zn^{2+} and proximal Ca^{2+} , pack against the substrate analogue, particularly at the S_2 subsite in this model. Thus, the bridging by divalent cations around the periphery of the sheet may be necessary to maintain the structure of the sheet and of one side of the active site cleft.

The active site zinc coordination by three histidyl nitrogen ligands was expected because of the homology with the zinc endopeptidase astacin, whose structure was solved (Bode et al., 1992). This was verified for collagenases by crystallography and for stromelysin by diagnostic imidazole chemical shifts (Gooley et al., 1993). The fourth ligand in uninhibited matrix metalloproteinases is expected to be a water molecule able to carry out nucleophilic attack on the scissile carbonyl once polarized by a conserved glutamate in helix B acting as a general base, like a mechanism proposed for thermolysin by Matthews (1988). Hydroxamate-substituted inhibitors like the one used in this study must displace this water in providing the fourth and fifth ligands.

Comparison with other MMP structures

The sequence similarity of stromelysin catalytic domain to crayfish astacin through three helices was pointed out earlier (Van Doren et al., 1993). The similarity of the tertiary structure of bacterial thermolysin with that of stromelysin catalytic domain has also been discussed by Gooley et al. (1994). In 1995, coordinates of a few matrix metalloproteinase structural models became available. The catalytic domains of human fibroblast collagenase and human stromelysin have 61% sequence identity when using the alignment of Whitham et al. (1986) and can be expected to have quite similar tertiary structures. A superimposition with the fibroblast collagenase crystallographic model of Lovejoy et al. (1994b; Protein Data Bank access code 1CGE) appears in Figure 8 and Kinemage 2. This figure shows that the

catalytic domains of these two respective matrix metalloproteinases superimpose quite well throughout the β -sheet and helices. When omitting the first eight residues of this NMR model of stromelysin (and the first six residues of the collagenase) because of the influence of conditions on the position of the collagenase N-terminus as discussed above, the pairwise RMSD for the backbone heavy atoms (N, CA, C', O) is 2.70 Å. (Structures were overlaid using Biosym's Insight II and RMSD calculated using the routine of Chris Ingalls.) The loop connecting β -strands III and IV superimpose poorly, partly because of a translation in the region of the calcium binding loop (see below). A three-residue insertion in stromelysin (Whitham et al., 1986) occurs in the long loop of irregular structure between helices B and C:

stromelysin:	229 T D L T R F R S L Q D D 238
collagenase:	G D V Q L A Q D D

When omitting 14 residues of the loop joining strands III and IV and 3 residues on each side of the insertion, the pairwise backbone RMSD improves to 2.28 Å.

The solution structure of stromelysin's catalytic domain reported by Gooley et al. (1994) was determined under conditions of lower calcium affinity (pH 5.5; see discussion above) and of lower calcium concentration (5 mM). The average backbone RMSD between five arbitrarily chosen members of the ensemble of Gooley et al. (1994) and five arbitrarily chosen members of our ensemble is 1.87 ± 0.3 Å. For comparison, the average pairwise backbone RMSD of one member of our ensemble from another member is about 1.3 Å. The superimposition of the structure of Gooley et al. and ours is also displayed in Figure 8. Most of the disparities between the model reported here and the models of Lovejoy et al. (1994b) and Gooley et al. (1994) occur in loops. In the solution structures, the loops are generally more poorly defined (Figs. 2, 3, 5) and more poorly re-

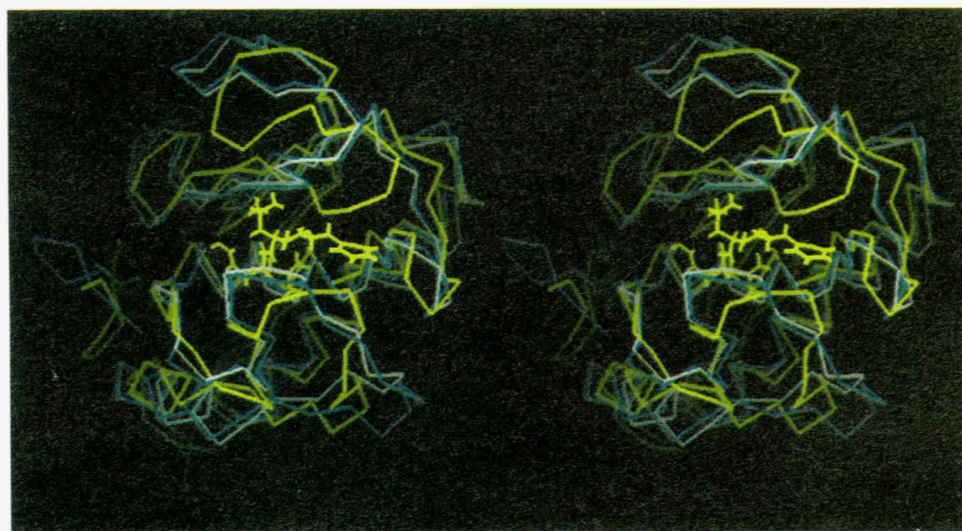


Fig. 8. Overlay of the current restrained average structure of stromelysin catalytic domain (yellow) with the X-ray crystallographic structure of collagenase catalytic domain (Lovejoy et al., 1994b; Protein Data Bank access code 1CGE, white) and the NMR structure of stromelysin catalytic domain as determined by Gooley et al. (1994; 1995 updated structure Protein Data Bank access code 2SRT, light-blue).

strained with NOEs (Fig. 4). The high degree of solvent exposure is largely responsible for this limitation on the number of NOE restraints. The solvent exposure limits the number of assignments because of higher amide proton exchange rates and because less groups are packed to yield NOEs. Mobility of the exposed loops may also reduce NOE intensity. The difficulty in obtaining complete aromatic assignments, particularly of phenylalanines, in proteins of this size is also a limitation. Such factors explain the limited number of NOEs in residues 149–156 of the loop joining β -strands III and IV, for example, and thus probably compromise the accuracy as well as the precision in underdetermined loop regions such as this. The calcium binding region of the loop between strands III and IV is, however, well defined in our solution model of stromelysin. This loop appears as a large S-shaped structure in the top right-hand half of Figure 8. Yet, a large difference exists in the position of this loop in our structure as compared to both the structures of Lovejoy et al. (1994b) and Gooley et al. (1994). This difference is a translation of 4–5 Å, whereas the conformation of the loop itself is approximately the same in the structures. In particular, the loop in our structure is much more closely packed against the inhibitor and against the loop in the region of residue number 190 (center right in Fig. 8). We list here several key NOEs that seem to dictate this difference: these are NOEs Asn 162 H α –Gly 192 HN and Val 163 methyl–Thr 193 H α , which are completely unambiguous by themselves and which are supported by several other NOEs (e.g., 161–193 and 160–193). In our average structure, the distances between the protons involved are 5.4 Å and 5.2 Å for the 162–192 and 163–193 NOEs, respectively. In contrast, the structure reported by Gooley et al. (1994) yields 16 and 12 Å for these distances. We must therefore conclude that a significant and major difference exists between the packing of this structural Zn/Ca loop against the protein in the different reported protein structures.

Bound substrate analogue

Though several stereoscopic views of inhibitors bound to fibroblast and neutrophil collagenases have been presented and some coordinates of the complexes have been more recently released (Bode et al., 1994; Borkakoti et al., 1994; Lovejoy et al., 1994a; Stams et al., 1994), only a single set of coordinates of a drug bound to stromelysin was available at the time of this writing. Recently determined structures show that when a substrate analogue is bound, it runs antiparallel to β -strand IV at the edge of the sheet. Most of the complexes, including the one reported here, have the substrate bound in the primed sites (C-terminal to the scissile bond) in an extended fashion. A hydroxylamine-substituted tripeptide complexed with neutrophil collagenase, however, binds to the unprimed sites, mimicking the N-terminal end relative to the scissile bond of a substrate (Bode et al., 1994). A substrate then can be expected to drape across the active site of a matrix metalloproteinase in an extended fashion. The portion of the stromelysin active site that a natural substrate would occupy should be from [N- to C-terminus] “northeast to southwest” in Figure 7. This swath is very hydrophobic, as represented by the green color of the Van der Waals surface. A significant fraction of substrate binding energy is therefore expected to arise from the interaction of the substrate hydrophobic side chains with this surface. That there may also be electrostatic contributions to the binding energy is suggested by the exchange-

protection of the amide protons of Tyr 223 and Ala 165 on opposite rims of the active site cleft even though these groups are not involved in canonical secondary structure hydrogen bonding patterns. Regrettably, the present definition of the structure is not sufficient to clearly identify the hydrogen bond acceptors that could be in the substrate analogue.

Starting at the “southwest” end at the P₃ position, the phenylalaninamide occupies a nook so shallow (S₃), it is questionable whether it is a subsite of any impact upon specificity or affinity. Indeed, the substrate specificity studies of Niedzwiecki et al. (1992) revealed a need for no residue, but perhaps a small hydrogen bond donor at the P₃ position. Figure 7 would suggest S₃ is somewhat hydrophilic. The P₃ position of the inhibitor (phenylalaninamide) is quite well defined despite the 2.4-Å pseudoatom corrections in the NOE restraints, because of the large number of the restraints. This is surprising because of the lack of a pocket at the S₃ subsite. The aromatic resonances of this P₃ phenylalaninamide are remarkably sharp, having an intrinsic line width of 8–10 Hz when subtracting away a 7-Hz contribution from scalar coupling. Most proton resonances of the protein are much broader, having widths of at least 20 Hz. This suggests the phenylalaninamide residue may actually experience a dynamic equilibrium between a conformation in which it packs against the protein and transiently builds up a number of NOEs and a state in which it is more freely moving and exposed to the solvent. Thus, the high precision of P₃ is likely to be an artifact of conventional structure calculation methods. Such dynamic behavior could possibly be better modeled with long trajectory molecular dynamics simulations using time-averaged NMR restraints, keeping in mind that the details of the dynamic model derived by such methods may be of limited value. Such an approach has accounted for discrepancies between high-resolution NMR and crystallographic models of chymotrypsin inhibitor 2 as the differing conformations satisfied restraints when averaging over time (Nanzer et al., 1994). We do not have any indication that other residues of the bound inhibitor are subject to similar averaging: their resonances are broad, and their intermolecular NOEs have similar intensities as protein intramolecular NOEs. The tightly bound state for the inhibitor as a whole inferred from these observations is in accordance with the measured macroscopic K_i of 10^{−7}–10^{−8} M (depending on substrate) at the solution conditions employed in this study (15% acetonitrile) (Q.-Z. Ye, unpubl.).

The S₂ subsite occupied by the leucine side chain is quite hydrophobic though open to the surface. The lack of definition of the P₂ leucine in the subsite is a consequence of the comparatively limited number of NOE assignments and of the large methyl-methyl pseudoatom correction in the restraints. The S₂ subsite appears to be a shelf broad enough to accommodate very bulky hydrophobic side chains. This agrees with the marked preference for phenylalanine or tryptophan at the S₂ subsite in both inhibition studies (Darlak et al., 1990; Kortylewicz & Galardy, 1990; Grobelny et al., 1992) and substrate specificity studies of homologous collagenase (Netzel-Arnett et al., 1991). Limited studies in stromelysin reveal a similar preference for tryptophan at S₂ as a determinant of specificity in inhibition (Ye et al., 1994) and in substrate hydrolysis (Niedzwiecki et al., 1992), again consistent with the site seen in Figure 7.

Thorough studies of stromelysin’s S₁ subsite specificity requirement show a clear preference for hydrophobic residues, particularly phenylalanine and leucine (Niedzwiecki et al., 1992).

They found the unbranched, unnatural amino acid norvaline in this site to be threefold more active than these. These observations are consistent with the depth and narrowness of the hydrophobic S₁' site seen in Figure 7. If ¹³C labeling of the inhibitor had been available to enable stereospecific assignments of its methyl groups, the definition of the P₁' *i*-butyl side chain in this deep pocket would still be better. The depth of the S₁' site has been reported in the crystallographic models of collagenase as well. Thus, the specificity studies qualitatively agree with the structural features of this stromelysin-inhibitor complex and may aid drug design.

We have compared the binding mode of the inhibitor in the current structure with that in the recently released stromelysin structure reported by Gooley et al. (1994). In both cases, the inhibitor binds in an extended conformation. The location of the P₁' side chain and the location of the S₁' pocket are identical in both structures. However, the position of the inhibitor backbone is moved further to the "front" of the molecule (in the view of Fig. 8) in our structure. This places the loop around Pro 221 (the lower "lip" of the binding cleft, see Fig. 8) significantly farther forward and lower. Although it is very difficult to distinguish cause and effect of conformational differences between structures, we note that the P2' leucyl side chain in our molecule, being hydrophobic, is more tucked into the S2' pocket than the arginyl side chain in the model reported by Gooley et al. This placement could cause the shift of the inhibitor forward. Alternatively, the large significant shift in the position of the structural Zn/Ca loop (see above) could also cause this change of active site, or, conversely, this particular inhibitor may induce the change in conformation of that loop. Not neglected as possible causes of the structural differences can be the differences in pH, Ca²⁺ ion concentration, and the presence of acetonitrile as a co-solvent. We, however, conclude that the structural differences cannot be dismissed as being caused by indetermination of the areas involved. Nor can they be easily brushed away by challenging the NOE data our structure is based on: several unambiguous NOEs define the position of the areas involved. Differences between the structures might thus reflect differences in interactions between the structural Zn/Ca loop and the active site cleft at different solvent conditions.

Methods

NMR data collection and handling

The stromelysin catalytic domain was expressed in *Escherichia coli* and purified from inclusion bodies as described previously by Ye et al. (1992). Preparation of the labeled samples, typically about 1 mM, and of the buffers (containing 10 mM Tris-*d*1-HCl, pH 7.0, 20 mM CaCl₂, 15% acetonitrile-*d*3 and 8% D₂O) was as described by Van Doren et al. (1993). The hydroxamate-substituted inhibitor (ICI U24522; DiPasquale et al., 1986) was present at a ratio of 1:1 with the protein for the half-filtered experiments (cf. Ikura & Bax, 1992). In all other experiments, the inhibitor concentration exceeded the protein concentration.

The cross-polarization-driven HCCH-TOCSY (HEHOHE HAHA; Majumdar et al., 1993), HSQC (Bodenhausen & Ruben, 1980), HCH (Yamazaki et al., 1993), HMQC-J (Kay & Bax, 1990), and gradient-enhanced NOESY-HSQC and HSQC-NOESY (Majumdar & Zuiderweg, 1993) spectra were acquired with an AMX500 spectrometer (Bruker Analytische Messtechnik

GMBH, Karlsruhe, Germany) equipped with a Bruker Grasp unit and triple resonance gradient probe. The CBCA(CO)NH (Grzesiek & Bax, 1992), HBHA(CO)NH (Grzesiek & Bax, 1993), ¹³C-resolved FSCT-HSMQC-NOESY (Van Doren & Zuiderweg, 1994), half-filtered NOESY, and filtered TOCSY (Bax et al., 1994) spectra were acquired on an AMX-600 equipped with an auxiliary fourth channel (Van Doren & Zuiderweg, 1993). Spectra were processed using Felix (Hare Research, Inc., Bothell, Washington) and interpreted using the Felixtalk interface for Felix (written by Dr. A. Majumdar).

Restraints

Interresidue NOE restraints involving amides were obtained from 3D [¹⁵N]NOESY-HSQC (Fesik & Zuiderweg, 1988; Marion et al., 1989; with modifications of Van Doren et al., 1993) and 3D [¹³C]HSQC-NOESY, both collected in H₂O using gradient enhancements (Majumdar & Zuiderweg, 1993) at 500 MHz with 70 ms mixing time. 3D [¹³C]FSCT-HSMQC-NOESY (Van Doren & Zuiderweg, 1994) in D₂O at 600 MHz with 55 ms τ_m , carrier at 76 ppm, and SUSAN-1 broadband decoupling scheme (Sunita Bai et al., 1994) was the principle source of NOE restraints among both aliphatic and aromatic groups. Assignments of the peptide-derived inhibitor relied on a TOCSY (35 ms mixing time) with ¹³C-bound protein protons suppressed using J cross-polarization (Bax et al., 1994) and on [F₁-¹²C, F₂-¹²C] NOESY with ¹³C-bound protons suppressed in both dimensions (Ikura & Bax, 1992), both recorded at 600 MHz using uniformly ¹³C/¹⁵N-labeled stromelysin complexed with an unlabeled hydroxamate-substituted peptide-like inhibitor in D₂O. At 600 MHz, 2D ¹³C-suppressing [F₁-¹²C] NOESY in D₂O and ¹³C/¹⁵N-suppressing [F₂-¹²C/¹⁴N] NOESY in H₂O (cf. Ikura & Bax, 1992), each with 100 ms mixing times, revealed NOEs between inhibitor and protein. An HMQC-J (Kay & Bax, 1990) provided ϕ angle restraints.

NOE distance restraints with 1.8-Å lower bounds were conservatively assigned upper bounds of 2.7 Å for very strong, 3.2 Å for strong, 4 Å for medium, or 5 Å for very weak NOEs. Participation of methyl groups pushed the restraint into the next larger bin. Conventional pseudoatom corrections (Wüthrich, 1986) were applied. Fifty-five ϕ torsion angles were loosely restrained using ranges of -160 to -80 for ³J_{HnH α} > 9 Hz, -170 to -70 for ³J_{HnH α} > 8 Hz, -180 to -60 for ³J_{HnH α} ~ 8 Hz provided d _{α N(i,i)} not strong, or -90 to -30 for ³J_{HnH α} < 6 Hz, similar to ranges used by Clubb et al. (1994). Forty-two hydrogen bonds (two restraints per bond) were included for slowly exchanging amides (present after 18 h at pH 7 at 32 °C) in the sheet and helices. The bounds for such amide protons to carbonyl oxygens were 1.5 and 2.3 Å, whereas the bounds for such amide nitrogens to oxygen were 2.5 and 3.3 Å in order to maintain linearity. Distance restraints between two zinc atoms and their histidyl nitrogen ligands (bounds of 1.95 and 2.25 Å), consistent with both the imidazole nitrogen assignments of Gooley et al. (1993, 1994) and with the ligands seen in the crystallographic structure of the homologous fibroblast collagenase crystallographic structure (Lovejoy, 1994a), were employed. Six calcium to oxygen distance restraints (to Asp 158 O δ 1, Asp 181 O δ 2, Glu 184 O ϵ 2 with bounds of 1.75 and 2.25 Å; to Gly 159 O, Gly 161 O, Val 163 O with bounds of 2.05 and 2.55 Å) were used in the model based on the structure of the homologous collagenase (Lovejoy et al., 1994a). The hydroxamate substituent

at the N-terminus of the peptidic inhibitor was modeled with a distance restraint (1.75 and 2.25 Å) from the catalytic Zn²⁺ to each of its oxygens in accordance with the crystallographic results for collagenases with hydroxamate inhibitors bound (e.g., Borkakoti et al., 1994; Stams et al., 1994). Omega torsion angle restraints were added to maintain *trans* planarity of the peptide bonds of non-proline residues.

Structure calculations and evaluation

Distance geometry was used to generate 39 starting structures then optimized by distance-driven dynamics (simulated annealing without a physical forcefield) using DGII (Havel, 1991; Biosym Technologies, Inc., San Diego, California). Using Discover (Biosym), the 39 structures were further refined using a simulated annealing protocol using the Amber forcefield without use of charges, followed by extensive restrained minimization. The 10 structures having the highest energy (sum of restraining and conformational terms) were removed from the ensemble. These 10 have some of the highest RMSDs from the other members of the ensemble, judging from pairwise RMSDs. Two more structures were culled on the basis of single large violations greater than 0.75 Å. Another seven structures were culled on the basis of unique, localized aberrations or conformational stresses in regions well defined in the other structures and were accompanied by an unusually large number of violations in these regions. Twenty of the 39 were accepted. These structures were superimposed using all backbone heavy atoms or all heavy atoms using InsightII (Biosym). The average structure was refined by extensive restrained minimization. Mean RMSD values to the average structure, residue by residue, were tabulated using software written by Chris Ingalls of Parke-Davis/Warner-Lambert Co. Angular order parameters (Hyberts et al., 1992) were calculated using routines provided by Dr. Sven Hyberts and an interface written by Chris Ingalls.

Coordinates

The atomic coordinates have been deposited with the Protein Data Bank. The ID codes are IUMS (an ensemble of 20 structures of stromelysin catalytic domain complexed with hydroxamate inhibitor ICI U24522) and IUMT (the energy minimized average structure).

Acknowledgments

This work was supported by NIH grant GM R01 52406-01 to E.R.P.Z and by American Cancer Society fellowship PF-4056 to S.R.V. We thank Drs. C.C. Humbel, M.D. Reily, and G.D. Glick for lending use of computer time for calculation of 24 of the starting structures in the time-consuming distance geometry step. We thank Mr. C. Ingalls for contributing RMSD analysis software and Dr. S.V. Hyberts for contributing scripts for measurement of angular order parameters. We acknowledge M.W.F. Fischer and H. Wang for software assistance. We appreciate stimulating discussions with Drs. H. Nagase, V. Thanabal, and A. Majumdar.

References

- Bax A, Grzesiek S, Gronenborn AM, Clore GM. 1994. Isotope-filtered 2D HOHAHA spectroscopy of a peptide–protein complex using heteronuclear Hartmann–Hahn dephasing. *J Magn Reson A* 106:269–273.
- Birkedal-Hansen H, Moore WGI, Bodden MK, Windsor LJ, Birkedal-Hansen B. 1993. Matrix metalloproteinases: A review. *Crit Rev Oral Biol Med* 4:197–250.
- Bode W, Gomis-Ruth FX, Huber R, Zwilling R, Stocker W. 1992. Structure of astacin and implications for activation astacins and zinc-ligation of collagenases. *Nature* 358:164–167.
- Bode W, Reinemer P, Huber R, Kleine T, Schnierer S, Tschesche H. 1994. The X-ray crystal structure of the catalytic domain of human neutrophil collagenase inhibited by a substrate analogue reveals the essentials for catalysis and specificity. *EMBO J* 13:1263–1269.
- Bodenhausen G, Ruben DJ. 1980. Natural abundance nitrogen-15 NMR by enhanced heteronuclear spectroscopy. *Chem Phys Lett* 69:185–189.
- Borkakoti N, Winkler FK, Williams DH, D'Arcy A, Broadhurst MJ, Brown RA, Johnson WH, Murray EJ. 1994. Structure of the catalytic domain of human fibroblast collagenase complexed with an inhibitor. *Nature Struct Biol* 1:106–110.
- Clavel C, Polette M, Doco M, Benninger I, Berembaut P. 1992. Immunolocalization of matrix metalloproteinases and their tissue inhibitors in human and mammary pathology. *Bull Cancer* 79:261–270.
- Clubb RT, Ferguson SB, Walsh CT, Wagner G. 1994. Three-dimensional solution structure of *Escherichia coli* periplasmic cyclophilin. *Biochemistry* 33:2761–2772.
- Darlak K, Miller RB, Stack MS, Spatola AF, Gray RD. 1990. Thiol-based inhibitors of mammalian collagenase. *J Biol Chem* 265:5199–5205.
- DiPasquale G, Caccese R, Pasternak J, Conaty J, Hubbs S, Perry K. 1986. Proteoglycan- and collagen-degrading enzymes from human interleukin-1 stimulated chondrocytes from several species; proteoglycanase and collagenase inhibitors as potentially new disease-modifying antiarthritic agents. *Proc Soc Exp Biol Med* 183:262–267.
- Fesik SW, Zuiderweg ERP. 1988. Heteronuclear three dimensional NMR spectroscopy; a strategy for the simplification of homonuclear two dimensional NMR spectra. *J Magn Reson* 78:588–593.
- Firestein GS, Paine MM. 1992. Stromelysin and tissue inhibitor of metalloproteinases gene expression in rheumatoid arthritis synovium. *Am J Pathol* 140:1309–1314.
- Gooley PR, Johnson BA, Marcy AI, Cuca GC, Salowe SP, Hagman WK, Esser OK, Springer JP. 1993. Secondary structure and zinc ligation of human recombinant short-form stromelysin by multidimensional heteronuclear NMR. *Biochemistry* 32:13908–13108.
- Gooley PR, O'Connell JF, Marcy AI, Cuca GC, Salowe SP, Springer JB, Johnson BA. 1994. The NMR structure of the inhibited catalytic domain of human stromelysin-1. *Nature Struct Biol* 1:111–118.
- Gravallese EM, Darling JM, Ladd AL, Katz JN, Glimcher LH. 1991. In situ hybridization studies of stromelysin and collagenase messenger RNA expression in rheumatoid synovium. *Arthritis Rheum* 34:1076–1084.
- Grobelny D, Poncz L, Galardy RE. 1992. Inhibition of human skin fibroblast collagenase, thermolysin, and *Pseudomonas aeruginosa* elastase by peptide hydroxamic acids. *Biochemistry* 31:7152–7154.
- Gronenborn AM, Clore GM. 1994. Identification of N-terminal helix capping boxes by means of ¹³C chemical shifts. *J Biomol NMR* 4:455–458.
- Grzesiek S, Bax A. 1992. Correlating backbone amide and side chain resonances in larger proteins by multiple relayed triple resonance NMR. *J Am Chem Soc* 114:6291–6293.
- Grzesiek S, Bax A. 1993. Amino acid type determination in the sequential assignment procedure of uniformly ¹³C/¹⁵N-enriched proteins. *J Biomol NMR* 3:185–204.
- Havel TF. 1991. An evaluation of computational strategies for use in the determination of protein structure from distance constraints obtained by nuclear magnetic resonance. *Prog Biophys Mol Biol* 56:43–78.
- Hu P, Ye QZ, Loo JA. 1994. Calcium stoichiometry determination for calcium binding proteins by electrospray ionization mass spectrometry. *Anal Chem* 66:4190–4194.
- Hyberts SG, Goldberg MS, Havel TF, Wagner G. 1992. The solution structure of eglin c based on measurements of many NOEs and coupling constants and its comparison with X-ray structures. *Protein Sci* 1:736–751.
- Ikura M, Bax A. 1992. Isotope-filtered 2D NMR of a protein-peptide complex study of a skeletal muscle myosin light chain kinase fragment bound to calmodulin. *J Am Chem Soc* 114:2433–2440.
- Kay LE, Bax A. 1990. New methods for the measurement of NH-CaH coupling constants in ¹⁵N-labeled proteins. *J Magn Reson* 86:110–126.
- Kortylewicz ZP, Galardy RE. 1990. Phosphoramidate peptide inhibitors of human skin fibroblast collagenase. *J Med Chem* 33:263–273.
- Kraulis P. 1991. MOLSCRIPT: A program to produce both detailed and schematic plots of protein structures. *J Appl Crystallogr* 24:946–950.
- Laskowski RA, MacArthur MW, Moss DS, Thornton JM. 1993. PROCHECK: A program to check the stereochemical quality of protein structures. *J Appl Crystallogr* 26:283–291.
- Li J, Brick P, O'Hare MC, Skarzynski T, Lloyd LF, Curry VA, Clark IM, Bigg HF, Hazleman BL. 1995. Structure of full-length porcine synovial

- collagenase reveals a C-terminal domain containing a calcium-linked, four-bladed β -propeller. *Structure* 3:541–549.
- Lovejoy B, Cleasby A, Hassell AM, Longley K, Luther MA, Weigl D, McGeehan G, McElroy AB, Drewry D, Lambert MH, Jordan SR. 1994a. Structure of the catalytic domain of fibroblast collagenase complexed with an inhibitor. *Science* 263:375–377.
- Lovejoy B, Hassell AM, Luther MA, Weigl D, Jordan SR. 1994b. Crystal structures of recombinant 19-kDa human fibroblast collagenase complexed to itself. *Biochemistry* 33:8207–8217.
- Majumdar A, Wang H, Morshauser RC, Zuiderweg ERP. 1993. Sensitivity improvement in 2D and 3D ¹³C HCC spectroscopy using heteronuclear cross-polarization. *J Biomol NMR* 3:387–397.
- Majumdar A, Zuiderweg ERP. 1993. Improved ¹³C-resolved HSQC-NOESY spectra in H₂O, using pulsed field gradients. *J Magn Reson B* 102:242–244.
- Marion D, Kay LE, Sparks SW, Torchia DA, Bax A. 1989. Three-dimensional heteronuclear NMR of ¹⁵N-labeled proteins. *J Am Chem Soc* 111:1515–1517.
- Matrisian LM. 1992. The matrix-degrading metalloproteinases. *BioEssays* 14:455–463.
- Matthews B. 1988. Structural basis of the action of thermolysin and related zinc peptidases. *Acc Chem Res* 21:333–340.
- Nagase H. 1995. Matrix metalloproteinases. In: Hooper NM, ed. *Zinc metalloproteases in health and disease*. Chichester, UK: Ellis Horwood.
- Nanzer AP, Poulsen FP, van Gunsteren WF, Torda AE. 1994. A reassessment of the structure of chymotrypsin inhibitor 2 (Cl-2) using time-averaged NMR restraints. *Biochemistry* 33:14503–14511.
- Neri D, Szyperski T, Ottign G, Senni H, Wüthrich K. 1989. Stereospecific nuclear magnetic resonance assignments of the methyl groups of valine and leucine in the DNA-binding domain of the 434 repressor by biosynthetically directed fractional ¹³C labeling. *Biochemistry* 28:7510–7516.
- Netzel-Arnett S, Fields G, Birkedal-Hansen H, Van Wart HE. 1991. Sequence specificities of human fibroblast and neutrophil collagenases. *J Biol Chem* 266:6747–6755.
- Niedzwiecki L, Teahan J, Harrison RK, Stein RL. 1992. Substrate specificity of the human matrix metalloproteinase stromelysin and the development of continuous fluorometric assays. *Biochemistry* 31:12618–12623.
- Okada Y, Shinmei M, Tanaka O, Naka K, Kimura A, Nakanishi I, Bayliss MT, Iwata K, Nagase H. 1992. Localization of matrix metalloproteinase 3 (stromelysin) in osteoarthritic cartilage and synovium. *Lab Invest* 66:680–690.
- Okada Y, Takeuchi N, Tomita K, Nakanishi I, Nagase H. 1989. Immunolocalization of matrix metalloproteinase-3 (stromelysin) in rheumatoid arthritis. *Ann Rheum Dis* 48:645–653.
- Reinemeyer P, Grams F, Huber R, Kleine T, Schnierer S, Piper M, Tschesche H, Bode W. 1994. Structural implications for the role of the N terminus in the “superactivation” of collagenases. *FEBS Lett* 338:227–233.
- Salowe SP, Marcy AI, Guca GC, Smith CK, Kopka IE, Hagmann WK, Hermes JD. 1992. Characterization of zinc-binding sites in human stromelysin-1: Stoichiometry of the catalytic domain and identification of a cysteine ligand in the proenzyme. *Biochemistry* 31:4535–4540.
- Sasaguri Y, Komiya S, Sugama K, Suzuki K, Inoue A, Morimatsu M, Nagase H. 1992. Production of matrix metalloproteinases 2 and 3 (stromelysin) by stromal cells of giant cell tumor of bone. *Am J Pathol* 141: 611–621.
- Shima I, Sasaguri Y, Kusukawa J, Yamaha H, Husita H, Hakeyawa J, Morimatsu M. 1992. Production of matrix metalloproteinase-2 and metalloproteinase-3 related to malignant behavior of esophageal carcinoma. *Cancer* 70:2747–2753.
- Stans T, Spurlino JC, Smith DL, Wahl RC, Ho TF, Qorofle MW, Banks TM, Rubin B. 1994. Structure of human neutrophil collagenase reveals large S1' specificity pocket. *Nature Struct Biol* 1:119–123.
- Stetler-Stevenson WG, Aznavoorian S, Liotta LA. 1993. Tumor cell interactions with the extracellular matrix during invasion and metastasis. *Annu Rev Cell Biol* 9:541–573.
- Sunitha Bai N, Kari N, Ramachandran R. 1994. An efficient windowless sequence for broadband heteronuclear decoupling. *J Magn Reson A* 106:241–244.
- Van Doren SR, Kurochkin AV, Ye QZ, Johnson LL, Hupe DJ, Zuiderweg ERP. 1993. Assignments for the main-chain nuclear magnetic resonances and delineation of the secondary structure of the catalytic domain of human stromelysin-1 as obtained from triple-resonance 3D NMR experiments. *Biochemistry* 32:13109–13122.
- Van Doren SR, Zuiderweg ERP. 1993. An auxiliary RF channel with convenient phase control for NMR spectrometers. *J Magn Reson A* 104: 222–225.
- Van Doren SR, Zuiderweg ERP. 1994. Improvements in HSMQC-type double- and triple-resonance NMR experiments by using full-sweep (semi-)constant-time shift labeling. *J Magn Reson B* 104:193–198.
- Walakots LA, Moore VL, Bhardwaj N, Gallick GS, Lark MW. 1992. Detection of stromelysin and collagenase in synovial fluid from patients with rheumatoid arthritis and posttraumatic knee injury. *Arthritis Rheum* 35:35–42.
- Wilhelm SM, Shao ZH, Housley TJ, Seperack PK, Baumann AP, Gunja-Smith Z, Woessner JF Jr. 1993. Matrix metalloproteinase-3 (stromelysin-1): Identification as the cartilage acid metalloproteinase and effect of pH on catalytic properties and calcium affinity. *J Biol Chem* 268:21906–21913.
- Whitham SE, Murphy G, Angel P, Rahmsdorf HJ, Smith BJ, Lyons A, Harris TJR, Reynolds JJ, Herrlich P, Docherty AJP. 1986. Comparison of human stromelysin and collagenase by cloning and sequence analysis. *Biochem J* 240:913–916.
- Woessner JF Jr. 1991. Matrix metalloproteinases and their inhibitors in connective tissue remodeling. *FASEB J* 5:2145–2154.
- Wüthrich K. 1986. *NMR of proteins and nucleic acids*. New York: John Wiley & Sons.
- Yamazaki T, Yoshida M, Nagayama K. 1993. Complete assignments of magnetic resonances of ribonuclease H from *Escherichia coli* by double- and triple-resonance 2D and 3D NMR spectroscopies. *Biochemistry* 32: 5656–5669.
- Ye QZ, Johnson LL, Hupe DJ, Baragi V. 1992. Purification and characterization of the human stromelysin catalytic domain expressed in *E. coli*. *Biochemistry* 31:11231–11235.
- Ye QZ, Johnson LL, Nordan I, Hupe D, Hupe L. 1994. A recombinant human stromelysin catalytic domain identifies tryptophan derivatives as human stromelysin inhibitors. *J Med Chem* 37:206–209.